ORIGINAL PAPER

Ion-selective PEDOT:PSS-decorated separator as a potential polysulfide immobilizer for lithium-sulfur batteries

Haritha Hareendrakrishnakumar[1] · Reshma Chulliyote[1] · Mary Gladis Joseph[1]

Abstract

PEDOT:PSS is one of the most investigated and broadly exploited conducting polymers with extensive applications. In this work, we present lithiated PEDOT:PSS-coated Celgard (Li$^+$-PEDOT:PSS@CG) separator for Li-S battery to alleviate the so-called shuttle effect, which is alleged to be a major bottleneck in Li-S chemistry. The Li$^+$-PEDOT:PSS@CG separator possesses a dual role, concurrently inhibit polysulfide shuttling and promote Li$^+$ selective diffusion. The negatively charged sulfonic acid groups present in PSS function as an electrostatic screen towards the soluble higher order polysulfides via coulombic repulsion, whereas the strong electronegative atoms (O and S) present in PEDOT render chemical interactions and form a chelated coordination structure with insoluble lithium sulfides. The dual shielding effect proffered by Li$^+$-PEDOT:PSS@CG effectively suppresses the polysulfide shuttling process by arresting the migrating polysulfides within the cathode compartment of the cell. Furthermore, the Li$^+$-PEDOT:PSS@CG membrane holds excellent electrolyte wettability, ionic conductivity and interfacial properties. The Li-S cell containing Li$^+$-PEDOT:PSS@CG separator unveiled substantial improvement in the electrochemical performance, suppressed polysulfide shuttling and anti-self-discharge properties. The cell displays an initial discharge capacity of 1096 mAh g^{-1} at 0.5C, and a capacity retention of 911 mAh g^{-1} over 500 cycles with an areal sulfur loading of 4.1 mg cm^{-2}.

Keywords Lithium-sulfur battery · Polysulfide shuttling · Modified separator · Lithiated PEDOT:PSS · Lithium ion selectivity

Introduction

The present lithium-ion technologies are still inadequate to satisfy the ever-increasing market exigencies of portable electronics, electrified transportation and grid storage applications [1, 2]. The rechargeable lithium-sulfur (Li-S) batteries have been envisaged as one of the most attractive alternatives for the next-generation energy storage systems due to its extremely high theoretical capacity (1675 mAh g^{-1}) and energy density (2600 Wh kg^{-1}) [3, 4]. Moreover, the low cost, abundance and environmentally benign nature of sulfur are added bonus for realizing the Li-S battery technology [5–7]. Regardless of these advantages, there are several technical challenges to this system that remain unresolved. First and foremost one is "polysulfide shuttle effect", which arises from the dissolution and diffusion of higher order polysulfide species (S$_x^{2-}$, 4 < x <

8) from the sulfur cathode to the lithium metal anode through the electrolyte medium [8–10] The polysulfide species reacts with the lithium metal to form lower order polysulfides which then migrates back towards the cathode side circuitously, which not only results in irreversible loss of active materials but also causes increase in interfacial resistance between anode and electrolyte, resulting in poor Coulombic efficiency and rapid capacity fading [11, 12].

Recently, researchers adopted various strategies to hinder the so-called shuttle effect in Li-S battery. The major strategies can be categorized into two aspects: cathode functionalization and separator modification [9, 13, 14]. Currently, modification of separator attained greater attention because of its ability to restrain the S$_x^{2-}$ within the cathode compartment either by physical hindrance and/or chemical bonding without affecting the utilization of active material [15, 16]. Therefore, modification of separator (polyolefin membranes like Celgard) with functionalized coatings (carbon, inorganic oxides and polymers) can be considered a reliable approach to achieve "shuttle-free" high-energy Li-S batteries [17, 18]. Among various functional coatings on separator, conducting polymers with functional groups are beneficial to reduce the interfacial

✉ Mary Gladis Joseph
marygladis@iist.ac.in; jmarygladis@gmail.com

[1] Department of Chemistry, Indian Institute of Space Science and Technology, Thiruvananthapuram 695 547, India

resistance along with alleviating the polysulfide diffusion towards anode compartment [19, 20]. Moreover, the commercial Celgard separators have a hydrophobic surface, which severely affects their electrolyte retention ability. Polymer coating on separator makes its surface hydrophilic, thereby improve the electrolyte uptake [21]. The presence of polar negative groups like $-SO_3^-$ and $-COO^-$ in the polymer chains not only suppresses S_x^{2-} crossover by Coulombic repulsion but also renders Li^+ permselectivity via Coulombic attraction. In addition, the presence of polar heteroatoms in the polymer shells imparts strong interactions with S_x^{2-} to build chemical bonds, thereby subdue the polysulfide dissolution [22, 23]. The separators modified with the polymers containing polar functional groups like nafion [24], polydopamine (PDA) [25], polyethylene glycol (PEG) [26], polyethylene oxide (PEO) [16], polyacrylic acid (PAA) [27], polyaniline (PANI) [28], polyacrylonitrile (PAN) [29], sulfonated polystyrene [30], sulfonated poly(styrene-ethylene-butylene-styrene) (SSEBS) [31], polyamide acid [32] poly(3,4-ethylenedioxythiophene):poly(styrene sulfonate) (PEDOT:PSS) [20, 33], sulfonated poly(ether ether ketone) (SPEEK) [34], carboxylate anchored polyvinyl alcohol [35] and poly(2-acrylamido-2-methyl-1-propanesulfonate) (PAMPS) [36] have proven efficient in improving electrochemical performance of Li-S battery. The separator coated with lithiated polymer acts as a single-ion conductor providing transport channels for Li^+, which further contributes to the performance of Li-S battery. The lithiated polymers like lithiated nafion [37], lithiated perfluorinated sulfonic acid [38], lithiated SSEBS [31], lithiated SPEEK [34] and lithiated PAMPS [36] have been investigated as barrier coatings to modify the commercial polyolefin separator. It has been reported that the lithiated polymers with polar negatively charged functional groups selectively enable the passage of positively charged Li^+ and abate the transit of negatively charged ions (S_x^{2-}) [39].

PEDOT:PSS is one of the most investigated and widely used conducting polymers with wide applications, especially as electrode material in various energy storage and conversion devices such as solar cells, supercapacitors, fuel cells, batteries and thermoelectric devices because it possesses a number of unique characteristics, such as solution-processability, high electrical conductivity (~ 4600 S cm^{-1}) and good chemical stability [40, 41]. PEDOT:PSS has been reported as conducting coating on sulfur cathode, functional separator coating and conductive binder to attain enhanced electrochemical performance in Li-S battery [20, 42, 43]. To the best of found knowledge, lithiated PEDOT:PSS has not been employed as a functional separator coating in Li-S battery. Herein, we present lithiated PEDOT:PSS-coated Celgard separator with dual role to concurrently inhibit polysulfide shuttling and promote Li^+ selective diffusion. The proton present in the sulfonic acid group of PEDOT:PSS is exchanged with lithium during lithiation and the resulted lithiated PEDOT:PSS (Li^+-PEDOT:PSS) holds Li^+ transport ability,

thereby serves as a single-ion conductor. In addition, lithiated form of the polymer is reported to be more effective than the commercially available form which is acidic due to acid side chains [21]. The Li^+-PEDOT:PSS coating on the cathode side of pristine Celgard separator (Li^+-PEDOT:PSS@CG) effectually eliminates the shuttling of polysulfides as a result of "electrostatic repulsion" effect offered by the negatively charged sulfonic acid groups (from PSS) and chemical interactions rendered by the strong electronegative atoms (from PEDOT). Consequently, the Li-S cell employing Li^+-PEDOT:PSS@CG displays excellent electrochemical performance and anti-self-discharge characteristics compared to the pristine Celgard separator (CG).

Experimental section

Synthesis of lithiated PEDOT:PSS

PEDOT:PSS (3.0–4.0% in H_2O) was procured from Sigma-Aldrich. Lithiation of PEDOT:PSS was performed through a simple ion-exchange process. One gram PEDOT:PSS solution was added to a solution of 0.1 M LiOH.H_2O (99.995% purity, Sigma-Aldrich) in double-distilled water. The resulted solution was stirred for 2 h at room temperature followed by vacuum drying at 80 °C for 24 h to obtain Li^+-PEDOT:PSS. The chemical formula and schematic illustration of the synthesis procedure of Li^+-PEDOT:PSS was given in Figure S1.

Preparation of Li^+-PEDOT:PSS-coated Celgard separator

Li^+-PEDOT:PSS was coated on the surface of Celgard separator using a doctor blade coating method. Briefly, 33 mg of poly(vinylidine fluoride) (PVDF), Mw $\sim 534,000$, Sigma-Aldrich) as binder was dissolved in 2 mL N-methyl-2-pyrrolidone (NMP, 99.5% purity, Sigma-Aldrich). Thirty-three milligrams of Li^+-PEDOT:PSS and 33 mg of super P carbon (Alfa Aesar) were added to this solution and the mixture was stirred for 5 h at room temperature to obtain a homogenous slurry. The obtained highly viscous slurry was coated onto one side of Celgard 2320 membrane (CG) and vacuum dried overnight at 60 °C. The presence of super P carbon helps to improve electronic conductivity and favour the adsorption of intermediate polysulfides, thereby hamper the serious shuttling mechanism in Li-S cell. The overall thickness of Li^+-PEDOT:PSS@CG separator was around 36 μm.

Fabrication of MWCNT-sulfur composite cathode

MWCNT-sulfur (MWCNT-S) composite was prepared by a facile melt-diffusion method, by which the melted sulfur (S,

99.998%, Sigma-Aldrich) could be impregnated into the MWCNT (95% purity, Sigma-Aldrich) matrix via capillary effect. Typically, elemental sulfur powder and MWCNT were homogeneously mixed in the weight ratio of 7:3 by manual grinding with a mortar and pestle. The homogenous mixture was then transferred into a sealed vessel and heated at 155 °C for 12 h under N_2 atmosphere. During this process, sulfur melts and had a lowest viscosity at 155 °C so that the molten sulfur could infuse into the 3D conductive network of MWCNT to obtain the MWCNT-S composite. To fabricate MWCNT-S composite cathode, a slurry containing 70 wt.% MWCNT-S composite (containing 66 wt.% of sulfur), 20 wt.% super P carbon and 10 wt.% PVDF binder in NMP solvent was and coated onto an aluminum foil using a doctor blade, dried in under vacuum at 60 °C for 12 h.

Material characterization

The lithiation of PEDOT:PSS was successfully confirmed by Fourier transform infrared spectra (FT-IR; PerkinElmer Spectrum 100) recorded in the selected spectral range of 2000–800 cm^{-1}. Zeta potential (Zetasizer Nano ZS, Malvern ZEN3600) of Li$^+$-PEDOT:PSS was measured in blank electrolyte (1:1 v/v DOL:DME) used for electrochemical evaluation. The surface morphology and chemical composition of the CG and Li$^+$-PEDOT:PSS@CG membranes were observed by field emission scanning electron microscopy (SEM; FEI Quanta FEG 200) equipped with energy-dispersive X-ray spectroscopy (EDS) and elemental mapping. The contact angle measurements were conducted at room temperature using the non-aqueous liquid electrolyte. The sulfur content in the MWCNT-sulfur composite cathode was calculated from thermogravimetric analysis (TGA; Hitachi STA7300 thermal analysis system) under N_2 atmosphere up to 800 °C with a heating rate of 10 °C min^{-1}.

Coin cell assembly

A standard 2032 type coin cell was assembled in an Ar-filled glove box (M Braun, Germany) employing MWCNT-S composite cathode with an areal sulfur loading of 3.9 mg cm^{-2} and lithium metal foil anode with electrolyte solution composed of 1 M LiN(CF$_3$SO$_2$)$_2$ (LiTFSI) in a mixture of DOL and DME (v/v = 1:1). The cells were assembled with CG and Li$^+$-PEDOT:PSS@CG separators. The electrolyte-to-sulfur (E/S) ratio was optimized to 6.4 µL/mg. Further addition of electrolyte results in electrolyte leakage while crimping and consequently damages the cell.

Electrochemical characterization

The ionic conductivity of CG and Li$^+$-PEDOT:PSS@CG membranes was measured by electrochemical impedance

measurements (Metrohm Autolab, Netherlands) assembling non-blocking cells comprised of stainless steel (SS)/membrane/SS (frequency range of 1 MHz to 50 mHz at various temperatures 0, 10, 20, 30, 40, 50, 60 and 70 °C).

The lithium ion transference number, t_{Li^+}, was calculated by the potentiostatic polarization technique employing a symmetric cell (Li/uncoated and coated Celgard/Li) at 25 °C using the formula

$$t_{Li^+} = \frac{I_{ss}(\Delta V - I_o R_o)}{I_o\ (\Delta V - I_{ss} R_{ss})} \tag{1}$$

where I_{ss} and I_o stands for the initial and steady-state current, respectively. The interfacial resistances, R_o and R_{ss}, were measured from EIS analysis before and after perturbation at 10 mV. The lithium ion diffusion coefficient, D_{Li^+}, was calculated from cyclic voltammogram according to the Randles-Sevcik equation.

$$I_p = 2.69 \times 10^5\ n^{1.5}\ A\ D_{Li^+}{}^{0.5}\ C_{Li}\ \vartheta^{0.5} \tag{2}$$

Here, I_p, n, A, C_{Li} and ϑ represents the peak current, the number of electrons transferred, area of the electrodes, concentration of lithium ions in the electrolyte and sweep rate, respectively.

Cyclic voltammetric (CV) and electrochemical impedance spectroscopic (EIS) analysis of the Li-S cells were performed by using a PGSTAT302N electrochemical workstation (Metrohm Autolab, Netherlands). The CV profiles were recorded at a scan rate of 0.1 mV s^{-1} in the potential range of 1.6 to 3.0 V versus Li$^+$/Li. The galvanostatic charge-discharge studies (BTS-4000, Newarelab) were performed between 1.6 and 3.0 V versus Li$^+$/Li at various currents. The calculation of specific capacity is based on the mass of sulfur in the cathode. The EIS measurements were performed at the open circuit voltage (OCV), with a perturbation potential of 10 mV in a frequency range of 0.1 to 10^5 Hz. The ionic conductivity of the CG and Li$^+$-PEDOT:PSS@CG membranes at different temperatures were evaluated using EIS sandwiching the membrane between two stainless steel blocking electrodes. The interfacial stability of membranes against lithium electrode was evaluated by the impedance response of symmetric Li/CG and Li$^+$-PEDOT:PSS@CG/Li cell at 25 °C as a function of time. Polysulfide shuttle current was measured for Li-S cell containing pristine CG and Li$^+$-PEDOT:PSS@CG at 2.3 V as described by Moy et al [41] The X-ray photoelectron spectroscopy (XPS, Physical Electronics, USA) analysis of lithium anode was done for the cells containing CG and Li+-PEDOT:PSS@CG after 100 cycles.

Polysulfide diffusion studies

The schematic representation of experimental setup used for visual polysulfide diffusion test is presented in Figure S2.

Li$_2$S$_6$ solution was prepared by mixing 4:3 molar ratio of Li$_2$S (99.98%, Sigma-Aldrich):elemental sulfur (99.998%, Sigma-Aldrich) in a solution of 1,3-dixolane (DOL) and 1,2-dimethoxyethane (DME) (v/v = 1:1) in an Argon filled glove box. The mixture was stirred at 50 °C for 12 h and the resulted brownish red solution corresponds to the average composition of Li$_2$S$_6$.

Results and discussion

PEDOT:PSS is a commercially available conductive polymer with chemical structure shown in Figure S1. PEDOT:PSS is available as aqueous dispersion consisting of a mixture of two ionomers: poly(3,4-ethylenedioxythiophene) (PEDOT) and polystyrenesulfonic acid (PSS). Among the constituent ionomers, PEDOT is water-insoluble in nature. The solubility issue associated with PEDOT is partially circumvented by the addition of a water-soluble polyelectrolyte, PSS during its polymerization. PSS also serves the role of a charge-balancing dopant, donating some of its protons to PEDOT to yield an aqueous dispersion of PEDOT:PSS. The PEDOT:PSS dispersion obtained from Sigma-Aldrich employed in this study is high conductivity grade (> 200 S cm^{-1}). To impart the property of lithium ion selectivity to PEDOT:PSS, the -SO$_3$H (from PSS) are lithiated using a simple ion-exchange procedure. FT-IR spectra were recorded to confirm the lithiation of PEDOT:PS. Figure 1 presents the FT-IR spectra of PEDOT:PSS and Li$^+$-PEDOT:PSS. Li$^+$-PEDOT:PSS displays analogous FT-IR bands to those of the pristine PEDOT:PSS. However, lithiation of PEDOT:PSS induces a shift in absorption band corresponding to the -SO$_3$H group of PSS towards the higher wavenumber (from 1241 cm^{-1} for PEDOT:PSS to 1287 cm^{-1} for Li$^+$-PEDOT:PSS). Such a shift in the absorption band mostly originates from
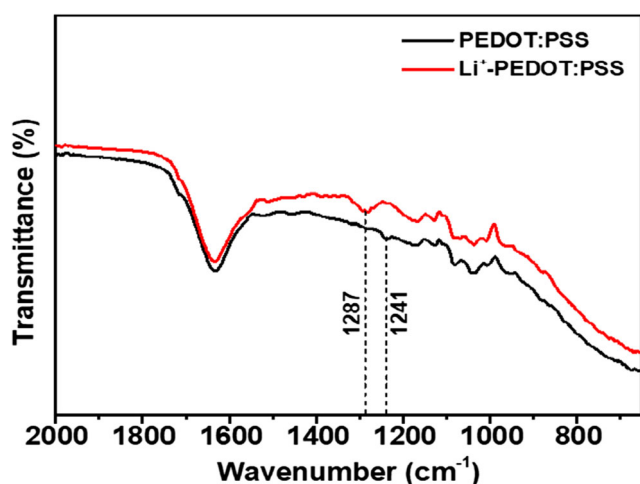

Fig. 1 FT-IR spectra of PEDOT:PSS and Li$^+$-PEDOT:PSS

the rupture of the -SO$_3$H bond, resulting in the formation of -SO$_3$Li [36–38].

The digital photographs of Li$^+$-PEDOT:PSS-coated commercial CG membrane is given in Fig. 2a, b. The excellent adhesion property of Li$^+$-PEDOT:PSS onto the CG membrane is illustrated by the folding test, as shown in Fig. 2c, d. The surface morphology of CG and Li$^+$-PEDOT:PSS@CG membranes was observed by SEM micrographs (Fig. 2e, f). As depicted in Fig. 2f, a dense coating of Li$^+$-PEDOT:PSS was wrapping the nanopores on the surface of CG. The conducting Li$^+$-PEDOT:PSS coating on the cathodic surface of the CG could physically obstruct the migration of polysulfide anions towards the anodic compartment and simultaneously augment the transport of lithium ions [20]. The elemental mapping of Li$^+$-PEDOT:PSS@CG (Fig. 2h) demonstrates uniformly distributed carbon, oxygen, sulfur and fluorine, which further confirms the fine dispersion of Li$^+$-PEDOT:PSS with super P and PVDF binder on the surface of CG. The cross-section SEM micrograph of Li$^+$-PEDOT:PSS@CG further exposes a dense structure with a thickness of ~ 34 μm (Fig. 2g).

The wettability of membranes with the electrolyte generally plays a vital role in determining the electrochemical performance of the Li-S cell such as Li$^+$ transportability and interface resistance [36, 44]. Figure 3 displays the static contact angle measurements with the sessile drop technique. The CG membrane exhibits a contact angle of 52.6° whereas the Li$^+$-PEDOT:PSS@CG membrane exhibits contact angle close to zero which indicate high wettability of the Li$^+$-PEDOT:PSS@CG with non-aqueous liquid electrolyte. The increased wettability of the Li$^+$-PEDOT:PSS@CG results from the presence of hydrophilic -SO$_3^-$ group on Li$^+$-PEDOT:PSS. The polar electrolyte droplet is immediately absorbed by the hydrophilic group (-SO$_3^-$) to build large clusters in the polymer domain, thereby increases the wettability of the separator [45, 46]. The wettability study affirms that the Li$^+$-PEDOT:PSS coating can attune the surface characteristics of CG and can lend hydrophilicity.

To validate the "electrostatic repulsion" effect offered by Li$^+$-PEDOT:PSS@CG membrane towards the polysulfide anions, zeta potential was measured for Li$^+$-PEDOT:PSS using blank electrolyte (1:1 v/v DOL:DME). The zeta potential of Li$^+$-PEDOT:PSS was found to be − 43.5 mV as shown in Figure S3, affirming the driving force between Li$^+$-PEDOT:PSS and lithium polysulfides. Since the polysulfides subsist as anionic in the electrolyte and Li$^+$-PEDOT:PSS is negatively charged, a repulsive force rises between Li$^+$-PEDOT:PSS and polysulfide anions [47]. Thus, Li$^+$-PEDOT:PSS coating can induce a permselective nature to the separator, thereby trapping the polysulfides within the cathode side, as illustrated in Scheme 1.

The PEDOT:PSS with abundant -SO$_3^-$ groups (from PSS) can confine the soluble lithium polysulfides (Li$_2$S$_n$, $4 \leq n \leq 8$)
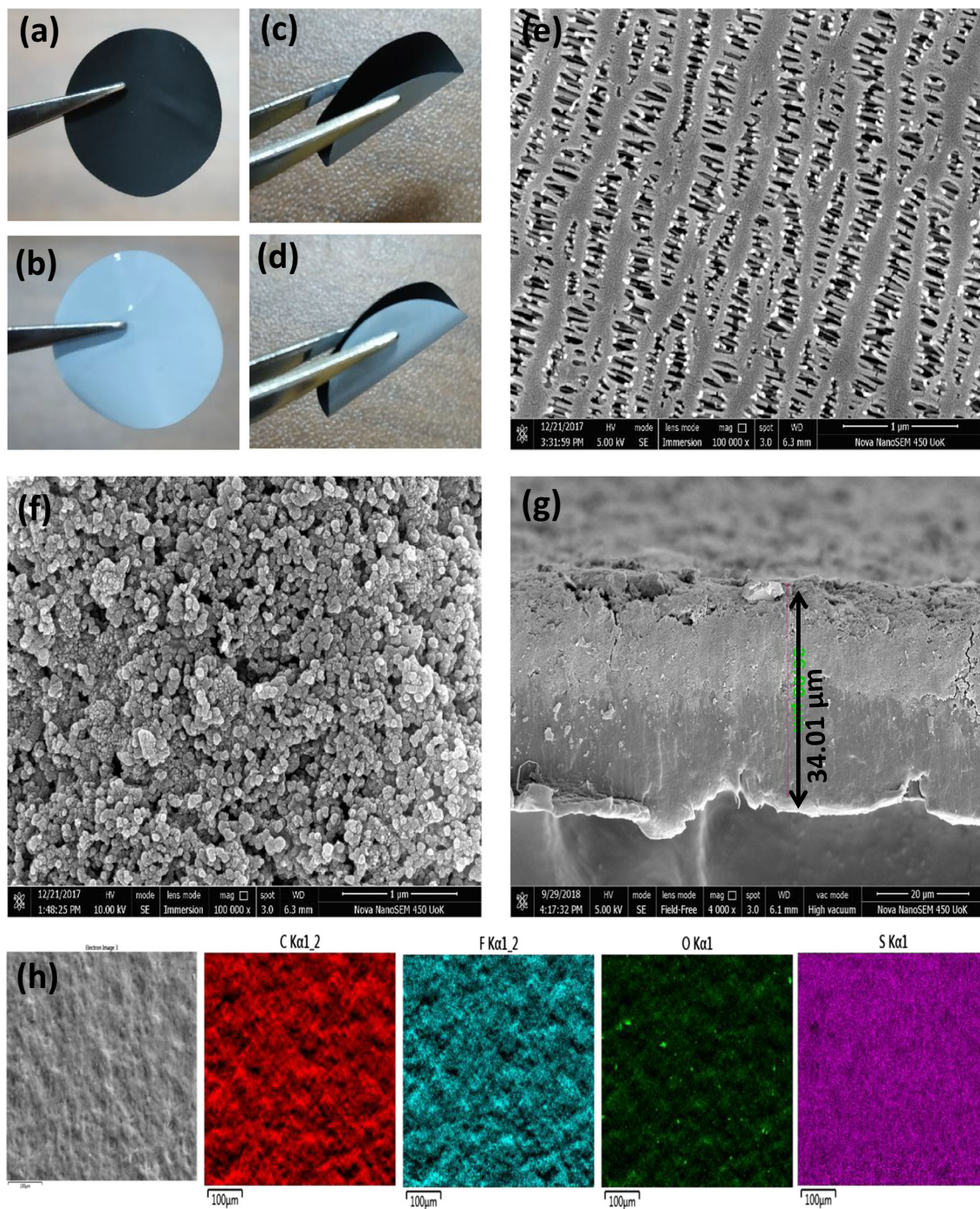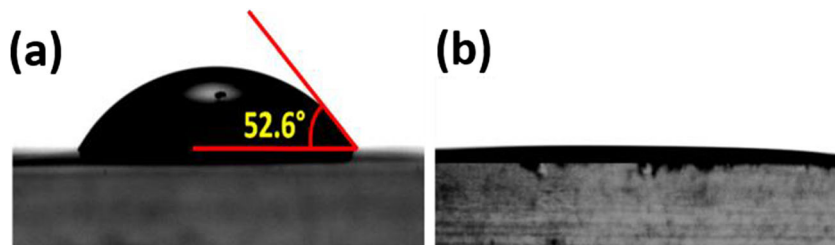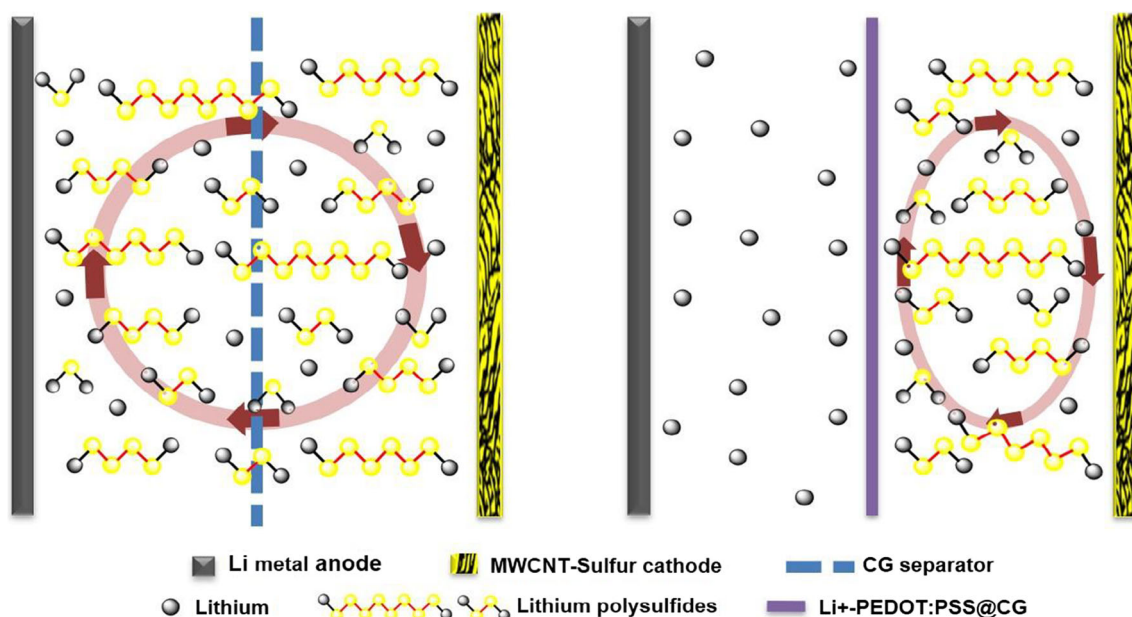
Fig. 2 Digital photographs of Li$^+$-PEDOT:PSS@CG membrane (a) coated side (b) uncoated side (c, d) folding test. SEM micrographs of (e) CG (f) Li$^+$-PEDOT:PSS@CG. (g) Cross-section SEM micrograph of Li$^+$-PEDOT:PSS@CG. (h) Elemental mapping of the Li$^+$-PEDOT:PSS@CG

**Fig. 3** Contact angle shots of (a) CG and (b) Li$^+$-PEDOT:PSS@CG

Scheme 1 Schematic configuration of Li-S cells with (a) CG separator, in which polysulfides shuttle between the cathode and anode side (b) Li$^+$-PEDOT:PSS@CG separator, in which the polysulfide anions are trapped within the cathode side

through mutual coulombic repulsion. On the contrary, the strong electronegative atoms (O and S) present in the PEDOT can bind strongly with insoluble lithium sulfides (Li$_2$S$_2$ and Li$_2$S) through coordination-like interactions among the lone pairs on electronegative atoms and the lithium present in Li$_2$S$_2$/Li$_2$S [33]. The existence of such Li-O and Li-S interactions is confirmed by using XPS analysis, which is identified to be extremely sensitive to the chemical environment [48]. It is clear from Fig. 4a that the Li1s XPS spectrum of pristine Li$_2$S can be fitted using a single peak with a binding energy of 55.2 eV, corresponding to Li-S bond. On the contrary, the Li1s spectrum of the Li$_2$S-PEDOT:PSS shows an asymmetric broadening towards higher binding energy (Fig. 5b), indicating a change in the chemical environment experienced by lithium. This Li1s spectrum can be fitted using two peaks: the peak at 55.3 eV corresponds to the Li-S bond, while the additional peak at 56.5 eV can be ascribed to Li-O interaction in the Li$_2$S-PEDOT:PSS [49].

To visually confirm the polysulfide rejection ability of CG and Li$^+$-PEDOT:PSS@CG membranes, polysulfide diffusion tests were conducted (Figure S4). With the passage of time, Li$_2$S$_6$ solution inside the small vial diffuses through the membrane into the blank electrolyte-bearing large vial [31] As foreseen, the pristine CG membrane could not restrain the polysulfides inside the small vial owing to its porous nature, consequently colourless blank electrolyte in the large vial turns into yellow over a period of 10 h. On the other hand, Li$^+$-PEDOT:PSS@CG membrane effectively hampers the polysulfide crossover, as we could not spot any yellow coloration in blank electrolyte even after a period of 50 h. The extraordinary polysulfide rejection ability of Li$^+$-PEDOT:PSS@CG could be ascribed to the coulombic repulsion provided by the negatively charged -SO$_3^-$ group present in Li$^+$-PEDOT:PSS [50].

The lithium ion conductivity as a function of inverse temperature for CG and Li$^+$-PEDOT:PSS@CG were measured and shown in Figure S5. Regardless of the membrane used,

Fig. 4 XPS spectra of the Li1s peak in (a) pristine Li$_2$S and (b) Li$_2$S-PEDOT:PSS, together with their respective fitted peaks
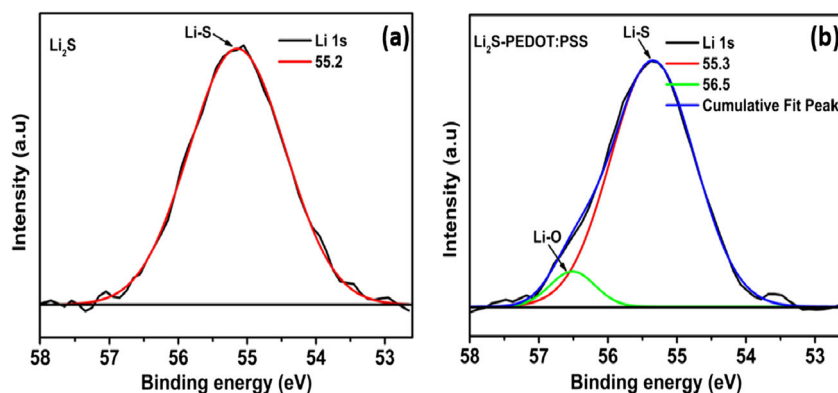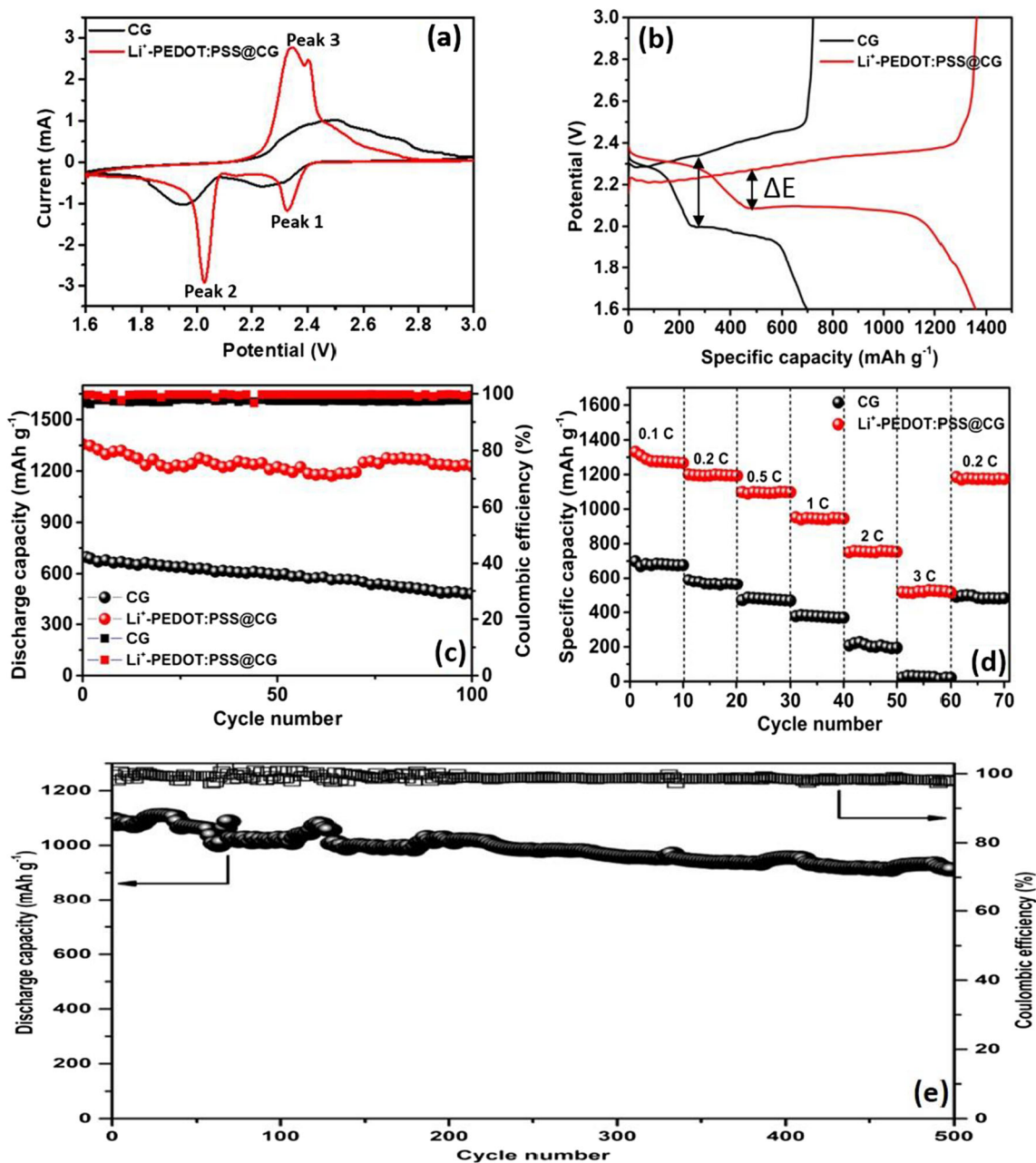
Fig. 5 (a) CV curves, (b) initial charge-discharge profiles, (c) the cycle performance and coulombic efficiencies of Li-S cells with CG and Li⁺-PEDOT:PSS@CG at 0.1C, (d) rate capability studies of Li-S cell with CG and Li⁺-PEDOT:PSS@CG, (e) the cycle performance and coulombic efficiencies of Li-S cell with Li⁺-PEDOT:PSS@CG at 0.5C

the ionic conductivity rises with rising temperature. The increased ionic conductivity of Li⁺-PEDOT:PSS@CG compared to CG membrane was accredited to the higher uptake of electrolyte by the hydrophilic -SO_3^- group present in the Li⁺-PEDOT:PSS coating [51]. The lithium ion transference number (t_+) was calculated from chronoamperometry and EIS analysis, employing Eq. (1). The chronoamperometric curves of Li/membrane/Li symmetric cells were recorded till it reached steady state and presented in Figure S6 (Inset: EIS spectra of the cells before and after DC polarization with a bias voltage of 10 mV) [52]. For Li⁺-PEDOT:PSS@CG separator,

the obtained t_+ value is 0.72, which is almost twofold higher than the CG separator (0.38). Lithium ions usually exist as solvated Li⁺-ether molecules in the ether-based electrolytes, which is much larger than TFSI⁻ ions. These larger solvated molecules suppress the transport of Li⁺, thereby relatively lower t_+ values [53]. Meanwhile, the high t_+ for the cells with Li⁺-PEDOT:PSS@CG can be ascribed to the -SO_3^- group present along the Li⁺-PEDOT:PSS chain, which is well-known for its ether coordination sites to promote the dissociation of Li⁺-ether molecules facilitating the transport of Li⁺ [35, 36]. In order to determine the interfacial stability of CG

and Li⁺-PEDOT:PSS@CG membranes with lithium metal, a symmetrical Li/membrane/Li cell was assembled and its interfacial resistance, R_i, was measured as a function of time at 25 °C and illustrated in Figure S7. The symmetric cell assembled with PEDOT:PSS@CG membrane demonstrated lowest R_i. This observation provides additional support to the earlier observations for ionic conductivity studies and t_{Li^+} calculations.

The electrochemical performance of Li-S cell with CG and Li⁺-PEDOT:PSS@CG membranes was evaluated by CV, galvanostatic charge-discharge and EIS measurements. Cyclic voltammograms of Li-S cells with CG and Li⁺-PEDOT:PSS@CG are shown in Fig. 5a. The cathodic sweep presents two peaks, one around 2.3 V (peak 1) and another around 2 V (peak 2). Peak 1 arises from the conversion of cyclo-S_8 to soluble higher order polysulfides (Li_2S_n, $4 \leq n \leq 8$). Peak 2 is the main peak in the cathodic sweep corresponding to the reduction of higher order polysulfides into lower order lithium sulfides (Li_2S_2/Li_2S), which will deliver significant portion of cell's capacity. During anodic sweep, a splitted oxidation peak is observed around 2.4 V (peak 3); the first peak is due to conversion of Li_2S_2/Li_2S to Li_2S_n (where $4 \leq n \leq 8$) and the next peak is due to further oxidation of Li_2S_n (where $4 \leq n \leq 8$) to S_8 [27, 31]. The cell with CG membrane displayed broad cathodic and anodic peaks due to the sluggish nature of the conversion kinetics [54]. In contrast, the cells with Li⁺-PEDOT:PSS@CG membrane presented well-defined redox peaks with an increased current density compared to the cells with CG membrane, indicating an improved conversion reaction kinetics and active material utilization [55].

Furthermore, diffusion coefficient of lithium ions (D_{Li^+}) was calculated from cyclic voltammogram using Eq. (2). The calculated values are tabulated in Table 1 and it is evident from the calculated values that diffusion coefficients for Li⁺-PEDOT:PSS@CG separator are at least one order of magnitude larger than CG. The above result suggests that the Li⁺-PEDOT:PSS@CG separator renders an improved Li⁺ transportability compared to pristine CG, thus anticipating substantial enhancement in the specific capacity and rate capability.

The initial galvanostatic charge-discharge profiles for Li-S cells containing CG and Li⁺-PEDOT:PSS@CG separator at 0.1C rate are shown in Fig. 5b. The plateaus observed in the

charge-discharge profiles correlates closely with the peak positions in the cyclic voltammogram. Two distinct plateaus are identified in the discharge profile, first one with upper plateau voltage corresponds to the reduction of cyclo-S_8 to soluble higher order PSs (Li_2S_n, $4 \leq n \leq 8$), which is a kinetically fast process. The second plateau at lower voltage results from the conversion of higher order polysulfides to Li_2S_2/Li_2S, which is a kinetically sluggish process contributing to nearly 75% of cell's capacity. The voltage hysteresis (ΔE) between the discharging and charging curve (at the second discharge plateau) for Li-S cells with CG and Li⁺-PEDOT:PSS@CG are 0.34 and 0.18 V, respectively, for the first cycle. The lower ΔE value for Li-S cell with Li⁺-PEDOT:PSS@CG indicates lower electrochemical polarization rooted from the improved ionic and electronic conductivity of the Li⁺-PEDOT:PSS coating layer. The high ionic conducting channels in Li⁺-PEDOT:PSS were offered by the sulfonate groups present in its chemical structure [56]. The absence of such ion-conducting functional groups in the case of pristine CG engenders an increased polarization, which in turn leads to decreased discharge capacity [57]. The Li-S cells containing CG and Li⁺-PEDOT:PSS@CG separator delivered an initial discharge capacity of 697 and 1357 mAh g⁻¹ with 41.6 and 81% sulfur utilization, respectively. The high initial discharge capacity of cells with Li⁺-PEDOT:PSS@CG is ascribed to good ionic conductivity of Li⁺-PEDOT:PSS coating, which provide a larger conductive surface for the conversion of soluble polysulfides to insoluble Li_2S_n ($n \leq 2$) [58].

Figure 5c compares the cycling performance and coulombic efficiency of Li-S cells containing CG and Li⁺-PEDOT:PSS@CG separators at a current density of 0.1C. It is clear from Fig. 5c that the Li-S cell assembled with Li⁺-PEDOT:PSS@CG provides higher discharge capacity than the cell assembled with CG membrane. The poor capacity retention exhibited by the Li-S cell assembled with CG (68% capacity retained after 100 cycles) might be due to the polysulfide shuttle effect, which occurs as a result of smooth passage of higher order polysulfides in the size range of 1–1.8 nm through the microporous CG separator towards the lithium metal anode. At the same time, the cell made of Li⁺-PEDOT:PSS@CG separator exhibits a capacity retention of 90.4% (1227 mAh g⁻¹) at 100th cycle. The high capacity retention noticed in the case of Li⁺-PEDOT:PSS@CG is attributed to the presence of -SO_3^- groups (from PSS) which impart PS repulsion ability together with the polar interaction of electronegative atoms (from PEDOT) with lower order lithium polysulfides [20, 34]. Besides, Fig. 5c shows an improvement in coulombic efficiency of Li-S cell when Li⁺-PEDOT:PSS@CG separator is employed. The high coulombic efficiency is an indirect indication of high ionic selectivity and low capacity loss [59]. The observed high coulombic efficiency arise from the permselectivity of Li⁺-PEDOT:PSS

Table 1 Lithium ion diffusion coefficients calculated for Li-S cells with CG and Li⁺-PEDOT:PSS@CG separator

D_{Li^+} (cm² s⁻¹)	CG	Li⁺-PEDOT:PSS@CG
Peak 1	4.84×10^{-7}	3.30×10^{-6}
Peak 2	1.09×10^{-7}	9.10×10^{-6}
Peak 3	4.71×10^{-7}	3.68×10^{-6}

coating, which selectively permeates lithium ions and effectively blocks the polysulfide anions.

The rate capability studies were conducted to compare the performance of Li-S cells with CG and Li⁺-PEDOT:PSS@CG separators at different current densities from 0.1 to 3C (Fig. 5d). Consequent cycles at 0.1, 0.2, 0.5, 1, 2 and 3C rates delivered capacities of 1336, 1196, 1099, 952, 750 and 520 mAh g⁻¹, respectively, for Li⁺-PEDOT:PSS@CG separator. When the C-rate was reverted back from 3C to 0.2C, a reversible capacity of 1170 mAh g⁻¹, i.e. 97.8% of the original capacity, was achieved. On the other hand, pristine CG separator provided discharge capacities of 699, 578, 485, 377, 199 and 36 mAh g⁻¹, respectively, at 0.1, 0.2, 0.5, 1, 2 and 3C. When the discharge current was switched back from 3 to 0.2C, a reversible capacity of 490 mAh g⁻¹, i.e. only 84.7% of the original capacity, was recovered. The excellent stability at different C-rates for Li-S cells with Li⁺-PEDOT:PSS@CG can be attributed to the effective confinement of polysulfides within the cathode compartment [20]. The cycling performance of Li-S cell with Li⁺-PEDOT:PSS@CG separator at 0.5C is shown in Fig. 5e. Over 500 cycles, a capacity retention of 83.1% (from 1096 to 911 mAh g⁻¹) is obtained, revealing its outstanding cycling stability. Furthermore, all the coulombic efficiencies maintain above 97%.

To gain additional insight into the influence of the Li⁺-PEDOT:PSS coating on the separator, EIS measurements were carried out for Li-S cells with CG and PEDOT:PSS@CG separator. These measurements were conducted for freshly prepared cells and cycled cells (after 100 cycles). The Nyquist plots displayed one or two semicircles in the high-to-medium frequency range and an inclined line in the lower frequency range (Fig. 6a, b). The high frequency intercept represents the bulk or solution resistance (R_e) of the cell, which includes resistance for ion transport in the electrolyte and cell components. A single semicircle displayed by Li-S cell with CG corresponds to the charge-transfer resistance (R_{ct}). At the same time, two discrete semicircles are presented by Li-S cell with Li⁺-PEDOT:PSS@CG; the first semicircle in the high frequency range is associated with the interface contact resistance (R_{int}) offered by the coating layer and

electrode bulk, while the second semicircle in the medium frequency range corresponds to the R_{ct} [60]. Based on the above discussion, we proposed an equivalent circuit model using ZSimpWin software as shown in the inset of Fig. 6a, b. In the proposed circuit model, $R_{int}//CPE_{int}$ is the interphase contact resistance and its related capacitance (Y_1 and n_1 are CPE_{int} elements). $R_{ct}//CPE_{dl}$ is the charge-transfer resistance and its related capacitance (Y_2 and n_2 are CPE_{dl} elements), which reflects the charge-transfer process at the interface between the conductive coating and the electrolyte. CPE_{dif} is the diffusion impedance (Y_3 and n_3 are CPE_{dif} elements), which represents lithium ion diffusion process [61].

Table 2 lists the fitted values for all of the equivalent circuit elements. It is evident from the fitted values for the equivalent circuit elements that the Li-S cell with Li⁺-PEDOT:PSS@CG exhibited reduced R_e and R_{ct} values than the cell with CG membrane. The considerably lowered R_{ct} value for the Li-S cell containing Li⁺-PEDOT:PSS@CG is conjoined with the enhanced lithium ion conductivity and electrolyte retention ability, which stem from the -SO₃⁻ groups present in the Li⁺-PEDOT:PSS coating [62]. Besides, the reduced R_{ct} value contributed to the enhanced electrode reaction kinetics [31]. Furthermore, a considerable reduction is observed in R_{int} and CPE_{dif} elements of the cycled cells with Li⁺-PEDOT:PSS@CG separator, which indicates better lithium ion diffusion ability. This is due to the reason that the Li⁺-PEDOT:PSS-coated separator can hold much more electrolyte within the separator facilitating fast ion transport [62]. The above EIS results can be deemed as a further support for the better cycling performance and rate capability offered by the Li-S cell assembled with Li⁺-PEDOT:PSS@CG separator.

The static electrochemical stability of Li-S batteries is usually expressed in connection with their self-discharge characteristics, which is an important parameter to be considered for both lab-scale testing and commercial applications [63]. In the case of Li-S battery, the self-discharge rate is considerably more than in conventional lithium-ion batteries and it leads to rapid capacity fading. The diffusion and side reactions of polysulfides with lithium metal anode are believed to be the

Fig. 6 Electrochemical impedance spectra of Li-S cells with (a) CG and (b) Li⁺-PEDOT:PSS@CG separators before and after cycling
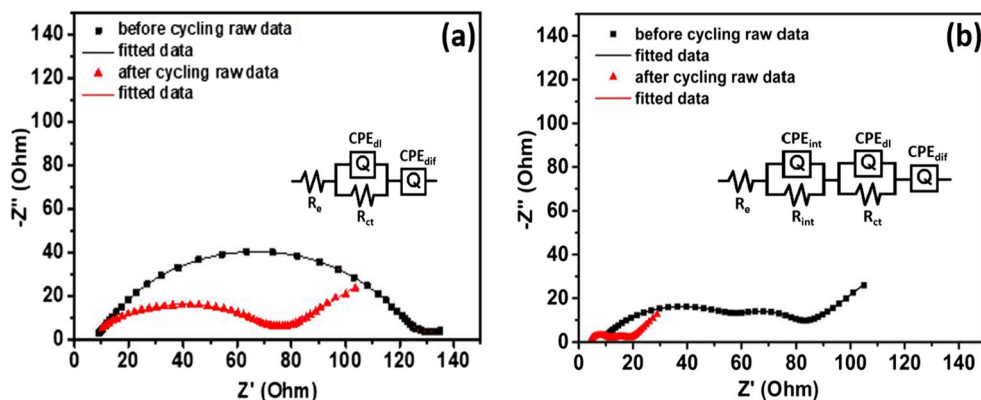
Table 2 Fitted values for the equivalent circuit elements by simulation of impedance spectra in Fig. 6a, b

	R_e (Ω)	CPE_{int}		R_{int} (Ω)	CPE_{dl}		R_{ct} (Ω)	CPE_{dif}	
		Y_1 ($\Omega^{-1}\,s^n$)	n_1		Y_2 ($\Omega^{-1}\,s^n$)	n_2		Y_3 ($\Omega^{-1}\,s^n$)	n_3
CG before cycling	9.53	-	-	-	9.09E−5	0.85	120.3	3.64E−2	0.61
CG after cycling	4.39	-	-	-	2.68E−5	0.80	72.14	3.45E−2	0.56
Li$^+$-PEDOT:PSS@CG before cycling	8.18	2.26E−5	0.87	54.48	4.04E−5	0.74	15.54	8.14E−2	0.56
Li$^+$-PEDOT:PSS@CG after cycling	3.97	6.31E−6	0.84	7.42	1.77 E−5	0.65	6.43	1.70E−2	0.49

major cause for high self-discharge rate in Li-S battery [64]. To evaluate self-discharge characteristics of Li-S cells containing CG and Li$^+$-PEDOT:PSS@CG separators, the OCV of the cells was monitored according to time and displayed in Figure S8a. The OCV of Li-S cell containing CG membrane swiftly drops to 2.14 V in 45 h, i.e.78.3% capacity retention, while the cell containing Li$^+$-PEDOT:PSS@CG maintained a high value of OCV (2.46 V) with a capacity retention of 87.2%. To gain an insight into the effect of self-discharge on cell's performance, the galvanostatic charge-discharge measurements were performed for Li-S cells containing CG and Li$^+$-PEDOT:PSS@CG separators [31]. After 10 continuous charge-discharge cycles, the cells were kept idle for 72 h, and then further cycled. During the first discharge after idle time (11th cycle), the cell containing pristine CG membrane exhibited a drastic decrease in capacity (Figure S8b), denoting apparent self-discharge. The second discharge after idle time (12th cycle) could restore only the partial capacity of the cell. Even during further cycling studies, the capacity loss occurred during idle condition could not be recovered completely. At the same time, the cell with Li$^+$-PEDOT:PSS@CG displays no obvious loss in discharge capacity even after the idle time, implying lower self-discharge.

Moy et al. have proposed a simple and straightforward approach to quantify the rate of shuttling process in Li-S batteries (termed as "shuttle current") by measuring the current flowing through the cell under potentiostatic control. Usually, the potential of a cell gradually decreases when kept idle due to the polysulfide shuttling mechanism. A Faradaic current was dispensed to control the polysulfide crossover in order to maintain a steady cell potential, which is measured as the shuttle current. The variation of shuttle current for Li-S cells containing CG and Li$^+$-PEDOT:PSS@CG membranes was measured at 2.3 V according to time (Fig. 7). The decline in the rate of shuttle current was acquired by linearly fitting the steady-state current region employing the equation $y = mx + C$, where y, x, C and m represents current, time, y-intercept and slope, respectively. The slope, m is an important parameter as it is a direct indication of the shuttle current decay [65]. It is clear from Fig. 7 that the cell containing Li$^+$-PEDOT:PSS@CG

membrane produced the nominal decay of current in course of time compared to the cell containing pristine CG membrane. The magnitude of shuttle current also trails the similar trend, i.e. the Li-S cell containing Li$^+$-PEDOT:PSS@CG displays lower shuttle current than the cell containing CG membrane. The reduction in shuttle current affirms the extensive elimination of polysulfide shuttling process, which further accord with the improved electrochemical performance and self-discharge characteristics of Li-S cells with Li$^+$-PEDOT:PSS@CG.

To further investigate the influence of Li$^+$-PEDOT:PSS@CG membrane in mitigating the polysulfide shuttle effect, the cycled Li-S cells (after 100 cycles) were decrimped in an Ar-filled glove box. The CG and Li$^+$-PEDOT:PSS@CG separators collected after decrimping the cells were used directly with no further washing treatment [47]. The surface morphology and elemental composition of both cathode and anode side of cycled separators were examined by SEM and EDS measurements. Compared with fresh separators (Fig. 2e, f), the cycled ones (cathode side) exhibit more dense structure with surface deposits (Figure S9a-b) arise out of accumulated polysulfides and electrolyte salts. The EDS results (Figure S9e-f) reaffirm above observation. The accumulated polysulfides on the separator will barely get involved
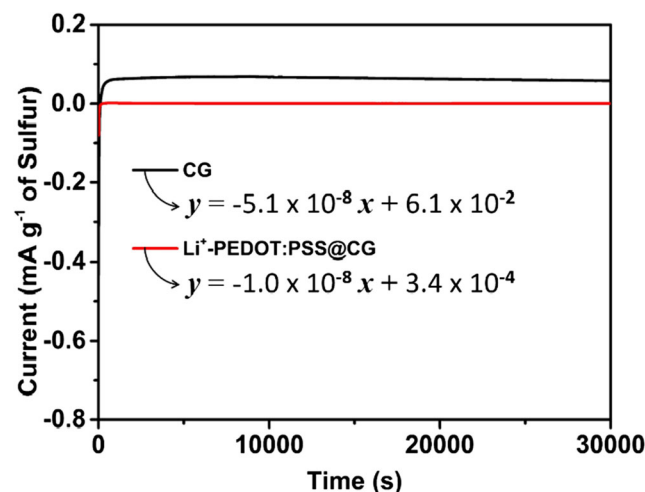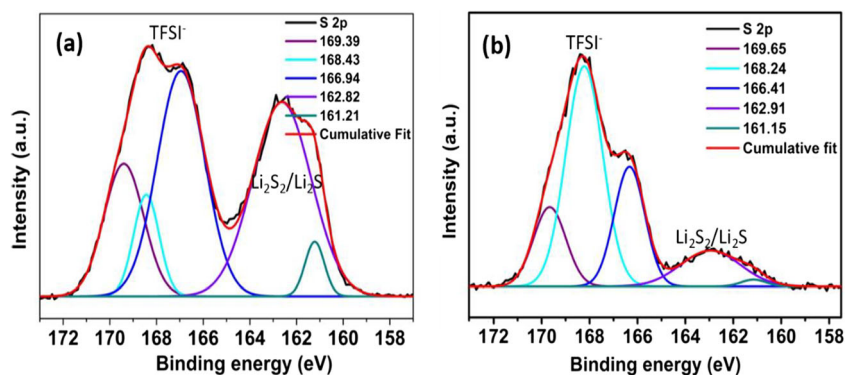

Fig. 7 Shuttle current measurements of cells containing CG and Li$^+$-PEDOT:PSS @CG membranes

Fig. 8 Deconvoluted S2p spectra for lithium anodes in the discharged state separated from the cells with (a) CG and (b) Li$^+$-PEDOT:PSS@CG membranes

in the redox reactions, which ultimately result in rapid capacity degradation of Li-S cell. Furthermore, this "dead sulfur" got arrested in the pores and the surface of CG and eventually blocks the lithium ion diffusion channels [66]. Figure S9c-d displayed the anode side SEM micrographs of pristine CG and Li$^+$-PEDOT:PSS@CG membranes. The effective confinement of polysulfides within the cathode chamber by Li$^+$-PEDOT:PSS coating offers a relatively clean anode side surface of the separator (Figure S9g-h).

The XPS analysis was conducted for lithium metal anodes peeled off from the two cells after 100 cycles. Figure 8 shows the deconvoluted S2p spectra for lithium anode obtained from Li-S cells with CG membrane (Fig. 8a) and Li$^+$-PEDOT:PSS@CG membrane (Fig. 8b). Both spectra present a broad peak at ~ 168 eV, that could possibly be due to the aerobic oxidation of sulfur species during dis-assembling the cell [67] The relatively low intensities of the deconvoluted peaks around 163 and 161 eV for Li$^+$-PEDOT:PSS@CG imply lower concentrations of polysulfides and Li$_2$S, respectively [68]. This observation strongly supports the proposed retention mechanism of polysulfide species within the cathode chamber for the cell with Li$^+$-PEDOT:PSS@CG separator.

Generally, the excellent cycling performance observed for the Li-S cells assembled with Li$^+$-PEDOT:PSS@CG separator could be accredited to the following reasons: (i) the negatively charged -SO$_3^-$ groups present in PSS encumber the shuttling of polysulfide anions, at the same time accelerating the transportation of Li$^+$ across the separator (ii) the strong electronegative atoms (O and S) present in PEDOT render chemical interactions and form a chelated coordination structure with insoluble lithium sulfides. Consequently, the Li$^+$-PEDOT:PSS coating on the separator offers dual shielding for migrating polysulfides. Table S1 compares the electrochemical performance of the Li-S cells fabricated with polymer-coated Celgard separators, with results from the literature and from this work. It is noteworthy that Li$^+$-PEDOT:PSS separator with excellent capacity and cycling stability outperforms other separator modification strategies adopted in literature. This suggests the potential of Li/Li$^+$-PEDOT:PSS@CG/MWCNT-S cell configuration in realizing a long cycle life Li-S battery.

Conclusion

In this chapter, we propose a novel approach of decorating commercial separator by bifunctional lithiated PEDOT:PSS (Li$^+$-PEDOT:PSS@CG). Owing to strong chemical interactions of PEDOT with insoluble lithium sulfides and the electrostatic repulsion between the negatively charged -SO$_3^-$ groups present in PSS and polysulfide anions, the Li-S cell (areal sulfur loading of 4.1 mg cm^{-2}) with Li$^+$-PEDOT:PSS@CG separator demonstrated a high initial discharge capacity of 1096 mAh g^{-1} and coulombic efficiency above 97%. It is notable that the Li$^+$-PEDOT:PSS@CG separator possesses excellent electrolyte wettability, interfacial properties and ionic conductivity, resulting in a stable discharge capacity of 911 mAh g^{-1} even after 500 cycles at 0.5C with 83.1% capacity retention. The excellent cycling stability exemplifies this facile method can effectively inhibit the polysulfide diffusion and ensure further progress towards the commercialization of Li-S batteries.

Compliance with ethical standards

Conflict of interest The authors declare that they have no conflicts of interest.

References

1. Gür TM (2018) Review of electrical energy storage technologies, materials and systems: challenges and prospects for large-scale grid storage. Energy Environ Sci 11:2696–2767
2. Cano ZP, Banham D, Ye S, Hintennach A, Lu J, Fowler M, Chen Z (2018) Batteries and fuel cells for emerging electric vehicle markets. Nat Energy 3:279–289
3. Manthiram A, Fu Y, Chung S-H, Zu C, Su Y-S (2014) Rechargeable lithium-sulfur batteries. Chem Rev 114:11751–11787

4. Shen X, Liu H, Cheng X-B, Yan C, Huang J-Q (2018) Beyond lithium ion batteries: higher energy density battery systems based on lithium metal anodes. Energy Storage Mater 12:161–175

5. Dong C, Gao W, Jin B, Jiang Q (2018) Advances in cathode materials for high-performance lithium-sulfur batteries. iScience 6:151–198

6. Salama M, Rosy RA, Yemini R, Gofer Y, Aurbach D, Noked M (2019) Metal–sulfur batteries: overview and research methods. ACS Energy Lett 4:436–446

7. Chulliyote R, Hareendrakrishnakumar H, Joseph MG (2019) Hierarchical porous carbon material with multifunctionalities derived from honeycomb as a sulfur host and laminate on the cathode for high-performance lithium–sulfur batteries. ACS Sustain Chem Eng 7:19344–19355

8. Hofmann A, Fronczek D, Bessler W (2014) Mechanistic modeling of polysulfide shuttle and capacity loss in lithium–sulfur batteries. J Power Sources 259:300–310

9. Ren W, Ma W, Zhang S, Tang B (2019) Recent advances in shuttle effect inhibition for lithium sulfur batteries. Energy Storage Mater 23:707–732

10. Mistry AN, Mukherjee PP (2018) "Shuttle" in polysulfide shuttle: friend or foe? J Phys Chem C 122:23845–23851

11. Wu F, Maier J, Yu Y (2020) Guidelines and trends for next-generation rechargeable lithium and lithium-ion batteries. Chem Soc Rev 49:1569–1614

12. Manthiram A, Fu Y, Su Y-S (2013) Challenges and prospects of lithium–sulfur batteries. Acc Chem Res 46:1125–1134

13. Fan X, Sun W, Meng F, Xing A, Liu J (2018) Advanced chemical strategies for lithium–sulfur batteries: A review. Green Energy Environ 3:2–19

14. He Y, Chang Z, Wu S, Zhou H (2018) Effective strategies for long-cycle life lithium–sulfur batteries. J Mater Chem A 6:6155–6182

15. Huang J-Q, Zhang Q, Wei F (2015) Multi-functional separator/interlayer system for high-stable lithium-sulfur batteries: progress and prospects. Energy Storage Mater 1:127–145

16. Rana M, Li M, Huang X, Luo B, Gentle I, Knibbe R (2019) Recent advances in separators to mitigate technical challenges associated with re-chargeable lithium sulfur batteries. J Mater Chem A 7:6596–6615

17. Kim MS, Ma L, Choudhury S, Archer LA (2016) Multifunctional separator coatings for high-performance lithium–sulfur batteries. Adv Mater Interfaces 1600450:3

18. Stoeck U, Balach J, Klose M, Wadewitz D, Ahrens E, Eckert J, Giebeler L (2016) Reconfiguration of lithium sulphur batteries: "enhancement of Li–S cell performance by employing a highly porous conductive separator coating". J Power Sources 309:76–81

19. Xiang Y, Li J, Lei J, Liu D, Xie Z-Z, Qu D, Li K, Deng T, Tang H (2016) Advanced separators for lithium-ion and lithium-sulfur batteries: a review of recent progress. ChemSusChem 9:3023–3039

20. Lee JH, Kang J, Kim S-W, Halim W, Frey MW, Joo YL (2018) Effective suppression of the polysulfide shuttle effect in lithium-sulfur batteries by implementing rGO-PEDOT:PSS-coated separators via air-controlled electrospray. ACS Omega 3:16465–16471

21. Dirlam PT, Glass RS, Char K, Pyun J (2017) The use of polymers in Li-S batteries: a review. J Polym Sci Part A: Polym Chem 55:1635–1668

22. Fang R, Zhao S, Sun Z, Wang D-W, Cheng H-M, Li F (2017) More reliable lithium-sulfur batteries: status, solutions and prospects. Adv Mater 29:1606823

23. Li C, Xi Z, Guo D, Chen X, Yin L (2017) Chemical immobilization effect on lithium polysulfides for lithium-sulfur batteries. Small 14:1701986

24. Bauer I, Thieme S, Brückner J, Althues H, Kaskel S (2014) Reduced polysulfide shuttle in lithium–sulfur batteries using Nafion-based separators. J Power Sources 251:417–422

25. Zhang Z, Zhang Z, Li J, Lai Y (2015) Polydopamine-coated separator for high-performance lithium-sulfur batteries. J Solid State Electrochem 19:1709–1715

26. Luo L, Chung S-H, Manthiram A (2016) A trifunctional multi-walled carbon nanotubes/polyethylene glycol (MWCNT/PEG)-coated separator through a layer-by-layer coating strategy for high-energy Li–S batteries. J Mater Chem A 4:16805–16811

27. Song S, Shi L, Lu S, Pang Y, Wang Y, Zhu M, Ding D, Ding S (2018) A new polysulfide blocker - poly(acrylic acid) modified separator for improved performance of lithium-sulfur battery. J Membr Sci 563:277–283

28. Chang C-H, Chung S-H, Manthiram A (2015) Ultra-lightweight PANiNF/MWCNT-functionalized separators with synergistic suppression of polysulfide migration for Li–S batteries with pure sulfur cathodes. J Mater Chem A 3:18829–18834

29. Zhu J, Chen C, Lu Y, Zang J, Jiang M, Kim D, Zhang X (2016) Highly porous polyacrylonitrile/graphene oxide membrane separator exhibiting excellent anti-self-discharge feature for high-performance lithium–sulfur batteries. Carbon 101:272–280

30. Guo Y, Sun M, Liang H, Ying W, Zeng X, Ying Y, Zhou S, Liang C, Lin Z, Peng X (2018) Blocking polysulfides and facilitating lithium-ion transport: polystyrene sulfonate@HKUST-1 membrane for lithium–sulfur batteries. ACS Appl Mater Interfaces 10:30451–30459

31. Yang K, Zhong L, Mo Y, Wen R, Xiao M, Han D, Wang S, Meng Y (2018) A functional separator coated with sulfonated poly(styrene-ethylene-butylene-styrene) to synergistically enhance the electrochemical performance and anti-self-discharge behavior of Li–S batteries. ACS Appl Energy Mater 1:2555–2564

32. Luo X, Lu X, Zhou G, Zhao X, Ouyang Y, Zhu X, Miao Y-E, Liu T (2018) Ion-selective polyamide acid nanofiber separators for high-rate and stable lithium–sulfur batteries. ACS Appl Mater Interfaces 10:42198–42206

33. Abbas SA, Ibrahem MA, Hu L-H, Lin C-N, Fang J, Boopathi KM, Wang P-C, Li L-J, Chu C-W (2016) Bifunctional separator as a polysulfide mediator for highly stable Li–S batteries. J Mater Chem A 4:9661–9669

34. Babu DB, Giribabu K, Ramesha K (2018) Permselective SPEEK/Nafion composite-coated separator as a potential polysulfide cross-over barrier layer for Li–S batteries. ACS Appl Mater Interfaces 10:19721–19729

35. Jiang K, Gao S, Wang R, Jiang M, Han J, Gu T, Liu M, Cheng S, Wang K (2018) Lithium sulfonate/carboxylate-anchored polyvinyl alcohol separators for lithium sulfur batteries. ACS Appl Mater Interfaces 10:18310–18315

36. Hareendrakrishnakumar H, Chulliyote R, Joseph MG, Suriyakumar S, Stephan AM (2019) Sulfonic groups stemmed ionic shield for polysulfides towards high performance Li–S batteries. Electrochim Acta 321:134697

37. Jin Z, Xie K, Hong X, Hu Z, Liu X (2012) Application of lithiated Nafion ionomer film as functional separator for lithium sulfur cells. J Power Sources 218:163–167

38. Shi Y, Wu C, Li L, Yang J (2017) A lithiated perfluorinated sulfonic acid polymer electrolyte for lithium-oxygen batteries. J Electrochem Soc 164:A2031–A2037

39. Lu W, Yuan Z, Zhao Y, Zhang H, Zhang H, Li X (2017) Porous membranes in secondary battery technologies. Chem Soc Rev 46:2199–2236

40. Sun K, Zhang S, Li P, Xia Y, Zhang X, Du D, Isikgor FH, Ouyang J (2015) Review on application of PEDOTs and PEDOT:PSS in energy conversion and storage devices. J Mater Sci Mater Electron 26:4438–4462

41. Ghosh S, Maiyalagan T, Basu RN (2016) Nanostructured conducting polymers for energy applications: towards a sustainable platform. Nanoscale 8:6921–6947

42. Lee J, Choi W (2015) Surface modification of sulfur cathodes with PEDOT:PSS conducting polymer in lithium-sulfur batteries. J Electrochem Soc 162:A935–A939

43. Pan J, Xu G, Ding B, Chang Z, Wang A, Dou H, Zhang X (2016) PAA/PEDOT:PSS as a multifunctional, water-soluble binder to improve the capacity and stability of lithium–sulfur batteries. RSC Adv 6:40650–40655

44. Suriyakumar S, Stephan AM, Angulakshmi N, Hassan MH, Alkordi MH (2018) Metal–organic framework@SiO2 as permselective separator for lithium–sulfur batteries. J Mater Chem A 6:14623–14632

45. Blake NP, Petersen MK, Voth GA, Metiu H (2005) Structure of hydrated Na−Nafion polymer membranes. J Phys Chem B 109: 24244–24253

46. Long L, Wang S, Xiao M, Meng Y (2016) Polymer electrolytes for lithium polymer batteries. J Mater Chem A 4:10038–10069

47. Lei T, Chen W, Lv W, Huang J, Zhu J, Chu J, Yan C, Wu C, Yan Y, He W, Xiong J, Li Y, Yan C, Goodenough JB, Duan X (2018) Inhibiting polysulfide shuttling with a graphene composite separator for highly robust lithium-sulfur batteries. Joule 2:2091–2104

48. Seh ZW, Wang H, Liu N, Zheng G, Li W, Yao H, Cui Y (2014) High-capacity Li2S–graphene oxide composite cathodes with stable cycling performance. Chem Sci 5:1396–1400

49. Liu Z, Borodin A, Li G, Liu X, Li Y, Endres F (2020) X-ray photoelectron spectroscopy probing of the interphase between solid-state sulfide electrolytes and a lithium anode. J Phys Chem C 124:300–308

50. Ahn JH, Shin H-J, Abbas S, Lee K-Y, Ha HY (2019) Plasma-functionalized carbon-layered separators for improved performance of lithium sulfur batteries. J Mater Chem A 7:3772–3782

51. Hencz L, Chen H, Ling HY, Wang Y, Lai C, Zhao H, Zhang S (2019) Housing sulfur in polymer composite frameworks for Li–S batteries. Nanomicro Lett 11:17

52. Karuppasamy K, Kim H-S, Kim D, Vikraman D, Prasanna K, Kathalingam A, Sharma R, Rhee HW (2017) An enhanced electrochemical and cycling properties of novel boronic ionic liquid based ternary gel polymer electrolytes for rechargeable Li/LiCoO2 cells. Sci Rep 7:11103

53. Zhou J, Guo Y, Liang C, Cao L, Pan H, Yang J, Wang J (2018) A new ether-based electrolyte for lithium sulfur batteries using a S@pPAN cathode. Chem Commun 54:5478–5481

54. Elgrishi N, Rountree KJ, McCarthy BD, Rountree ES, Eisenhart TT, Dempsey JL (2018) A practical beginner's guide to cyclic voltammetry. J Chem Educ 95:197–206

55. Ghosh S, Basu RN (2018) Multifunctional nanostructured electrocatalysts for energy conversion and storage: current status and perspectives. Nanoscale 10:11241–11280

56. Moorthy B, Kwon S, Kim J-H, Ragupathy P, Lee HM, Kim DK (2019) Tin sulfide modified separator as an efficient polysulfide trapper for stable cycling performance in Li–S batteries. Nanoscale Horiz 4:214–222

57. Puthirath AB, Baburaj A, Kato K, Salpekar D, Chakingal N, Cao Y, Babu G, Ajayan PM (2019) High sulfur content multifunctional conducting polymer composite electrodes for stable Li-S battery. Electrochim Acta 306:489–497

58. Yao H, Yan K, Li W, Zheng G, Kong D, Seh ZW, Narasimhan VK, Liang Z, Cui Y (2014) Improved lithium–sulfur batteries with a conductive coating on the separator to prevent the accumulation of inactive S-related species at the cathode–separator interface. Energy Environ Sci 7:3381–3390

59. Wang D, Zhang Z, Hong B, Lai Y (2019) Self-sacrificial organic lithium salt enhanced initial Coulombic efficiency for safer and greener lithium-ion batteries. Chem Commun 55:10737–10739

60. Lai F, Zhang X, Wang H, Hu S, Wu X, Wu Q, Huang Y, He Z, Li Q (2016) Three-dimension hierarchical Al2O3 nanosheets wrapped LiMn2O4 with enhanced cycling stability as cathode material for lithium ion batteries. ACS Appl Mater Interfaces 8:21656–21665

61. Deng Z, Zhang Z, Lai Y, Liu J, Li J, Liu Y (2013) Electrochemical impedance spectroscopy study of a lithium/sulfur battery: modeling and analysis of capacity fading. J Electrochem Soc 160:A553–A558

62. Zhang H, Zhao H, Khan MA, Zou W, Xu J, Zhang L, Zhang J (2018) Recent progress in advanced electrode materials, separators and electrolytes for lithium batteries. J Mater Chem A 6:20564–20620

63. Wang J, Yamada Y, Sodeyama K, Chiang CH, Tateyama Y, Yamada A (2016) Superconcentrated electrolytes for a high-voltage lithium-ion battery. Nat Commun 7:12032

64. Shen C, Xie J, Zhang M, Andrei P, Hendrickson M, Plichta EJ, Zheng JP (2019) Self-discharge behavior of lithium-sulfur batteries at different electrolyte/sulfur ratios. J Electrochem Soc 166:A5287–A5294

65. Moy D, Manivannan A, Narayanan SR (2015) Direct measurement of polysulfide shuttle current: a window into understanding the performance of lithium-sulfur cells. J Electrochem Soc 162:A1–A7

66. Kong L, Peng H-J, Huang J-Q, Zhu W, Zhang G, Zhang Z-W, Zhai P-Y, Sun P, Xie J, Zhang Q (2017) Beaver-dam-like membrane: a robust and sulphifilic MgBO2(OH)/CNT/PP nest separator in Li-S batteries. Energy Storage Mater 8:153–160

67. Lang X, Leow WR, Zhao J, Chen X (2015) Synergistic photocatalytic aerobic oxidation of sulfides and amines on TiO2 under visible-light irradiation. Chem Sci 6:1075–1082

68. Cao Y, Zuo P, Lou S, Sun Z, Li Q, Huo H, Ma Y, Du C, Gao Y, Yin G (2019) A quasi-solid-state Li–S battery with high energy density, superior stability and safety. J Mater Chem A 7:6533–6542

Publisher's note Springer Nature remains neutral with regard to jurisdictional claims in published maps and institutional affiliations.